Chinese Journal of Polymer Science Vol. 34, No. 3, (2016), 344–358

Chinese Journal of Polymer Science
© Chinese Chemical Society
Institute of Chemistry, CAS
Springer-Verlag Berlin Heidelberg 2016

Further Understanding on the Three Domains of Isotactic Polypropylene by Investigating the Crystalline Morphologies Evolution after Treatment at Different Domains*

Ding-ding Hu, Shi-bing Ye, Fei Yu and Jia-chun Feng**

State Key Laboratory of Molecular Engineering of Polymers, Collaborative Innovation Center of Polymers and Polymer Composite Materials, Department of Macromolecular Science, Fudan University, Shanghai 200433, China

Abstract The introduction of concept of the three domains of isotactic polypropylene (*i*PP) by Wittmann and Lotz *et al*. is an important advance in understanding the influence of the melt structures on the crystallization behaviors and consequent properties. To further understand the physical nature of the melt structures, the crystalline structures of *i*PP after thermal treatment in the three domains are systematically investigated. It is found that after treated at different domains the crystal morphologies, including the sizes and birefringence of spherulitic, the proportion of radial and tangential lamellae, *etc*., have distinctly different features. Our study reveals that the "nuclei" at domain II compose of locally ordered chains and the induced memory effect could not be erased under annealing treatment, while the "nuclei" at domain III compose of crystal fragments, which will aggregate under annealing process. Based on our results, highly schematic diagrams are proposed to illustrate the probable physical characteristics of the melt structures at the three different domains.

Keywords: Polypropylene; Self-nucleating; Annealing; Crystallization morphology.

Electronic Supplementary Material Supplementary material is available in the online version of this article at http://dx.doi.org/10.1007/s10118-016-1745-0.

INTRODUCTION

In practical thermoplastic processing, the molten states of semicrystalline polymers have significant influence on their crystallized multi-scale structures. Unlike the molten state of small molecules, polymer melt may preserve a strong memory of the pristine crystalline state. In light of different molten states as processing temperatures reduce from high to low, they will induce noticeable effects on the subsequent crystallization process[1]. Thus, to establish the relationship between melt structures and consequent properties is extremely important. Several decades ago, Wittmann and Lotz *et al*. divided the melt structures of isotactic polypropylene (*i*PP) into three temperature domains, *i.e.* domains I, II and III[2]. Domain I is defined as the range of temperatures high enough to completely melt all crystals, allowing the molecular chains to crystallize from amorphous phase with the lowest peak crystallization temperature (T_c). The temperature range of domain II decreases to the extent that survival "nuclei" are left in polymer melt, which increase the density of nucleation sites and accelerate the crystallization kinetics with a prominently increased T_c. Thus, domain II is also called self-nucleation (SN)

* This work was financially supported by the National Natural Science Foundation of China (Nos. 21174032 and 21574029) and China National Petroleum Corporation. We also greatly thank for the beam time provided by beamline BL16B1 of Shanghai Synchrotron Radiation Facility (Z14sr0051).
** Corresponding author: Jia-chun Feng (冯嘉春), E-mail: jcfeng@fudan.edu.cn
Received September 12, 2015; Revised October 7, 2015; Accepted October 23, 2015
doi: 10.1007/s10118-016-1745-0

domain. Domain III locates in the lowest temperature range where partial melting occurs and crystal annealing predominates. Since the concept of the three domains is put forward, many studies have been carried out to explore the relationship between the melt structures and crystallization behaviors in the last several decades. Based on the application of SN and annealing steps, some techniques have been developed for practical use, such as successive self-nucleation and annealing (SSA)[1, 3–7]. SSA is an important thermal fractionation protocol, which has been widely implemented to characterize the heterogeneous nature of the chain structure of polymers[4, 8–11]. By optimizing the choice of first SN temperature within domain II, a correct thermal fractionation result can be obtained[11–13]. Considering the significant influence of different melt structures on the final properties of *i*PP and the important application of thermal fractionation technology, further study the physical nature of the three domains is of great importance and remains a key issue for both academy and industry.

Over the past decades, various characterization techniques, such as differential scanning calorimetry, optical microscope and rheological measurements, have been applied to study the three domains of polymers. The features of the three domains, *e.g.* the domain II phenomena of elevated crystallization temperature and domain III phenomena of double melting peaks, have been intensively investigated[5, 6, 14–16]. Müller *et al*. summarized a schematic diagram to illustrate at a molecular level the different self-nucleation domains (see Ref. [13]) and considered two possibilities of melt status in domain II. At higher temperature end of domain II, the melt retains some residual segmental orientation and at the lower end, small crystal fragments survive and constitute self-nuclei. However, the details of the melt states at the three domains are still under debate, and how the melt states influence the formation of consequent crystal morphologies lacks systematic studies. As is widely known, variations in the applied thermal treatments, including the SN temperature T_s and the time τ_s spent at T_s, will lead to various melt structures. These melt structures significantly influence the crystallization behaviors afterwards, which in turn implies that we can speculate the variations in their original molten situation through the observation of final morphologies[3, 16–19]. Therefore, the investigation of the microstructure evolutions after different thermal treatments provides a good opportunity to grasp the physical nature of the three domains, which may also help us clarify some controversies such as whether the crystal fragments exist in the melt and how the crystals evolve under different melt states.

In the present report, we carried out a systematic investigation on the physical characteristics of melt structures at the three domains by carefully observing the crystalline morphologies, lamellae thickness and populations of radially/tangentially oriented lamellae, *etc*., of *i*PP, after being treated at various melting temperatures. Based on our results, we clarify some characteristics of "nuclei" remaining at each domain and present a phenomenological model to depict the physical nature and characteristics of polymer melt in the three domains.

EXPERIMENTAL

A commercially available polypropylene (F401), was purchased from Yangzi Petrochemcal Co. (China) with melt flow index of 2.5 g/10min (230 °C /2.16 kg). Thermal treatments were carried out by using a Q2000 DSC (TA Instruments, USA). The main SN thermal protocol is schematically shown in Fig. 1. Step (a): hold the samples at 200 °C for 5 min to erase previous thermal history and create the "standard" sample by cooling from 200 °C to 30 °C at a rate of 10 K/min. Step (b): complete or partial melting is achieved by heating the "standard" samples to T_s at a rate of 10 K /min and holding at T_s for a given time τ_s. Step (c): the samples recrystalized from T_s to 30 °C at a rate of 10 K/min and are labeled in the uniform format; for example, "S168-10" means the sample has been thermally treated at 168 °C for 10 min. Step (d): heat the resultant samples to 200 °C at a rate of 10 K/min, recording the re-melting curves.

The morphological photographs of crystallization were captured by a DM2500P polarized optical microscope (POM) (Leica, Germany) equipped with a THM600 hot-stage (Linkam, U.K.). The vector direction of the polarizer was kept perpendicular to that of the depolarizer. An optical compensating plate was installed to

judge the positive or negative birefringence of the spherulites. All samples were thermally treated at the given T_s for τ_s and then cooled down to room temperature at 10 K/min to reproduce the conditions employed in DSC as described in the previous steps (a)–(c). Through the birefringence types of spherulites, we can estimate the proportions of radially and tangentially oriented lamellae.

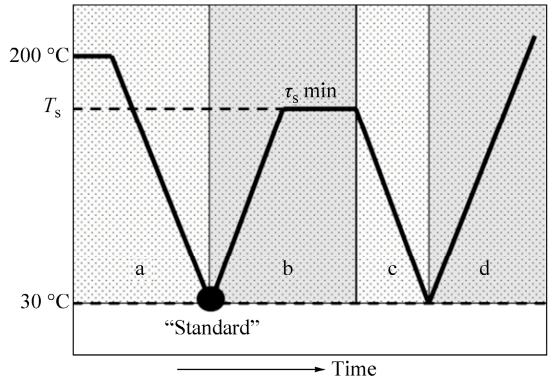


Fig. 1 Schematic diagram of the thermal procedures applied in the DSC

The microstructure morphologies of self-nucleated samples, including lamellae and spherulites structures, were characterized by an Ultra 55 field-emission scanning electron microscope (FESEM) (Zeiss, Germany) with an accelerating voltage of 3 kV. In order to exactly associate the crystallization morphologies in FESEM images and their exothermic/endothermic behaviors in DSC curves, all the samples for FESEM were prepared by using DSC. After the samples completed the thermal procedure of steps (a)–(c), they were etched for 12 h with an etchant containing 1.3 wt% potassium permanganate ($KMnO_4$), 32.9 wt% concentrated sulfuric acid (H_2SO_4), and 65.8 wt% concentrated phosphoric acid (H_3PO_4), according to the method proposed by Olley *et al.*[20] and then sputter-coated with gold before FESEM characterization.

RESULTS AND DISCUSSION

Three Domains of iPP Determined by DSC

The initial "standard" *i*PP is melted at 200 °C for 5 min to totally erase thermal history and cooled from 200 °C at 10 K/min. Through the procedure of complete or partial melting of the "standard" *i*PP at T_s for a given time τ_s, the SN experiences were systematically carried out by DSC to determine the temperature ranges of three domains. Considering the T_c and T_m detected by DSC are kinetics controlled, all the DSC measurements in this work are conducted at the same cooling/heating rate of 10 K/min. We choose τ_s = 5 min as the duration time, which is commonly used for most SN procedures[13]. Figure 2(a) shows the crystallization curves of *i*PP after thermally treated at different T_s, and Fig. 2(b) shows the respective re-melting curves. As can be seen, T_c of "standard" sample is 112.5 °C and the peak melting temperature T_m is about 162.5 °C. When T_s is above 171 °C, the crystallization and re-melting curves coincide with that of the "standard" sample and no memory effect is detected upon the cooling run with the unchanged T_c = 112.5 °C. It indicates that complete melting persists down to 171 °C, the temperature range of which is defined as domain I. When T_s is down to 170.5 °C, T_c dramatically shifts to 117.7 °C, which increases by nearly 5 K than that of the "standard" sample. Meantime, the melting peak (T_{m1}) slightly shifts to higher temperatures. It means the thermal treatment at 170.5 °C for 5 min is able to self-nucleate *i*PP. The pronounced increase of T_c is due to the residual "nuclei" in the melt, indicating typical feature of domain II. When T_s decreases to 166.5 °C, partial melting occurs along with the appearance of high temperature shoulder (T_{m2}) at 176.4 °C and double crystallization peaks in DSC curves. This extra endotherm, also called "annealing peak", becomes apparent as T_s decreases, which is peculiar to domain III.

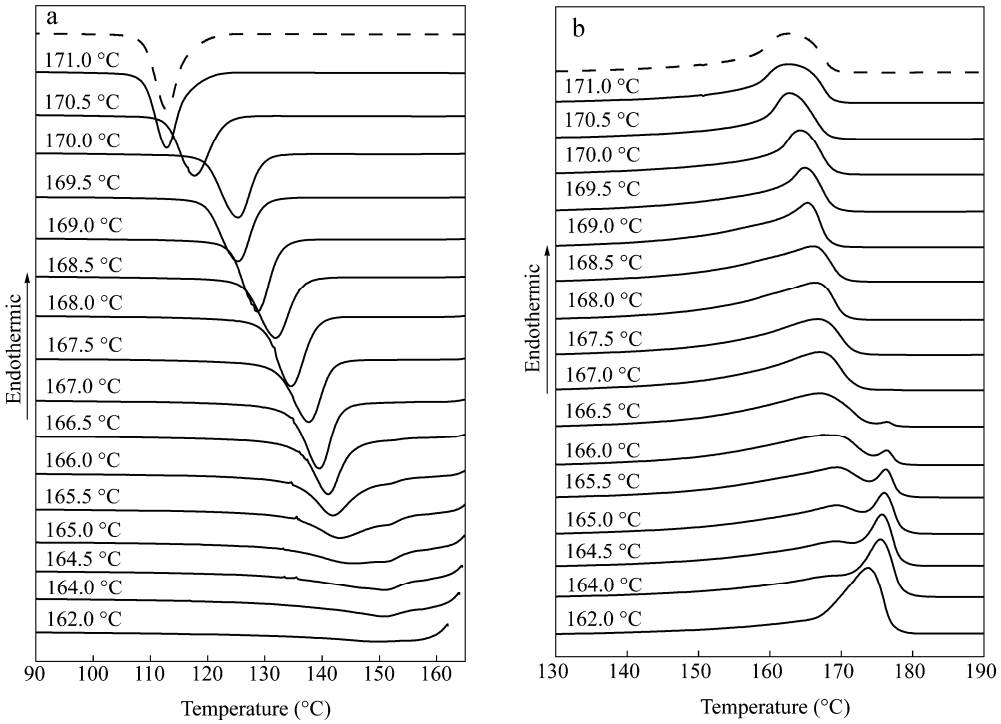


Fig. 2 (a) Crystallization curves of *i*PP after treated at various T_s as τ_s = 5 min; (b) Subsequent melting curves (Dash lines are the curves of "standard" sample for comparison.)

It needs to be careful to define the frontier between domains II and III since the observation of this annealing peak depends on the sensitivity of detector. When T_s locates in the upper range of domain III, where it closely adjoins to domain II, the residual crystal fragments in the melt are too scarce to be detected, showcasing the pseudo characteristic of domain II. For the example of *i*PP thermally treated at 167 °C for 5 min (S167-5), its re-melting curve only shows a main endothermic peak, the temperature of which might be classified into domain II. However, when τ_s is increased to 15 min, double endothermic peaks are emerging in the melting run (Fig. 3b),

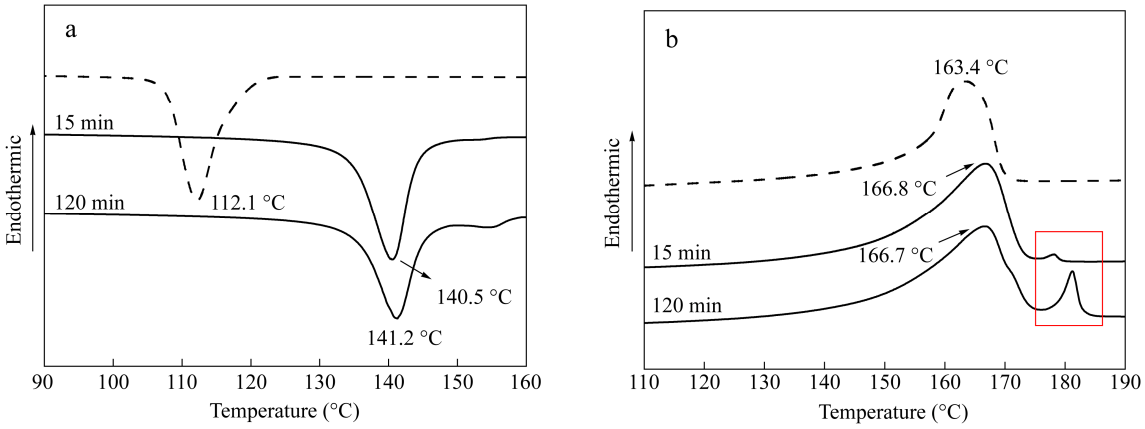


Fig. 3 (a) Crystallization curves of *i*PP after treated at 167 °C for 15 and 120 min; (b) Subsequent melting curves (Dash lines are the curves of "standard" sample for comparison.)

which is a convincing proof that T_s is in domain III, instead of domain II. As τ_s is prolonged to 120 min, double crystallization peaks are observed in the cooling process (Fig. 3a) and the annealing peak becomes much more evident (Fig. 3b), the phenomena of which are the typical features of domain III. Actually, the annealing peak in DSC melting curve of S167-5 does already exist, but is too weak to be observed. Based on the DSC results, the temperature range of domain II is determined between 171 °C and 167 °C and domain III is below 167 °C.

Morphology Features of iPP Crystallized from Three Domains

By utilizing POM and FESEM, the crystalline morphologies after thermal treatments in the three domains, particularly the birefringence patterns in crystallized spherulites and lamellae morphologies, are probed in detail. Generally, the lamellae in a spherulite are oriented either radially or approximately tangentially. According to Binsbergen *et al*., the refractive indices of the α-modification n_a, n_b and n_c belong to directions of polarization along the reciprocal *a* axis, the *b* axis and *c* axis; the birefringence is approximately $\Delta n = (n_c - n_a)(t - r/2)$, where *t* and *r* are corresponding to the fractions of tangential (T-) and radial (R-) lamellae[21]. Equipped with an optical compensating plate, POM can usually be used to distinguish the birefringence types of spherulites, positive, negative and mixed[22–25]. Although most lamellae do not lie exactly radially or tangentially, the relative amounts of R- and T-lamellae can be estimated through the observed sign of birefringence[26–30]. As reported by Hosier *et al*., the spherulites developed at the highest and lowest undercoolings show negative birefringence, which are due to a reduced frequency of T-lamellae, while most spherulites developed at intermediate undercooling show mixed birefringence[31]. Judged from the positive and negative birefringent spherulites, we can study the relative proportion of R- and T-lamellae of each sample to some extent. Figure 4 displays the formation of "standard" sample as temperature cooling from 200 °C. When temperature is cooling down to 125 °C, very few spherulites of *i*PP are formed. The initially growing spherulite in Fig. 4(a) shows that red and blue color randomly distribute in the spherulite, which indicates a mixed type of birefringence. During cooling process, the spherulite grows to a large size and still remains mixed birefringent, and the central part has a much higher birefringence than the remainder of the spherulite (Fig. 4b). The final spherulites of "standard" *i*PP crystallizes from 200 °C display a mixed birefringence as shown in Fig. 4(c). The mixed type of birefringence suggests a comparable proportion of R- and T- lamellae in spherulites.

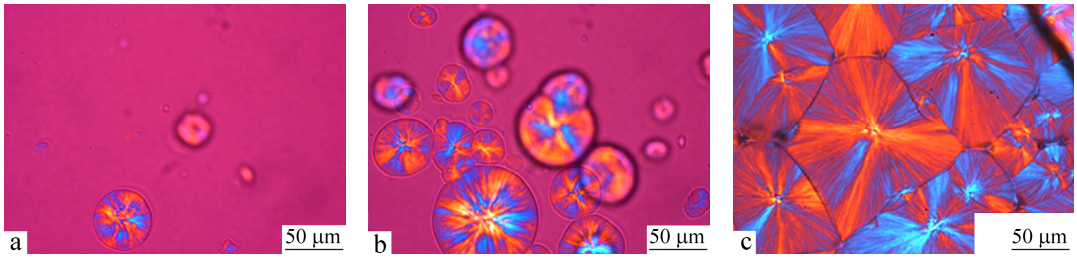


Fig. 4 POM images of "standard" sample crystallized from 200 °C at a cooling rate of 10 K/min: (a) the initial formation of spherulites when cooling down to 122 °C, (b) at 118 °C and (c) the final morphology

After "standard" *i*PP is thermally treated at domain I, for instance 200 °C for 5 min (S200-5), large spherulites with mixed birefringence are observed, as shown in Fig. 5(a), which is similar with that of "standard" sample (Fig. 4c). The similarity should be ascribable to the fact that the "standard" sample and the sample crystallized from domain I both have erased the thermal history. Furthermore, we use FESEM to obtain the lamellae texture within a spherulite on the micro level. After etching, large spherulites of S200-5 are clearly visible (Fig. 5b) and the details of the lamellae structures are magnified in Fig. 5(c). The spherulites contain spindly R-lamellae and many short T-lamellae around R-lamellae, showing a clear texture of typical cross-hatching structure. The thickness of R- and T-lamellae is approximately 22 and 13 nm, respectively. The thicker R-lamellae than the T-lamellae may result from that molecules within the T-lamellae include higher density of defects, which will consequently induce the less perfect crystallization of T-lamellae than R-lamellae[32].

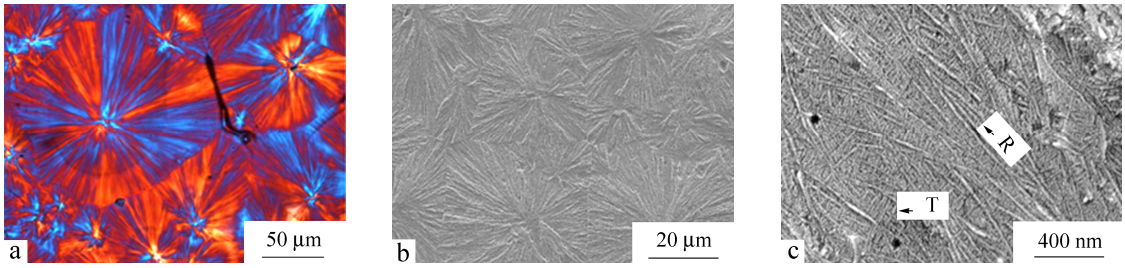


Fig. 5 Crystalline morphologies of *i*PP after treated at 200 °C for 5 min (S200-5): (a) POM image; (b) and (c) FESEM images with different magnifications

As T_s enters domain II, SN occurs with a prominently increased T_c, because some "nuclei" retain in the melt. When T_s is chosen in the upper range of domain II, for instance, after thermally treated at 169.5 °C for 5 min (S169.5-5), we cannot observe large spherulitic patterns clearly in POM (Fig. 6a). However, in Fig. 6(b), the spherulitic pattern is still visible but the size has shrinked dramatically to ~10 μm, far smaller than that in S200-5 (~80 μm, Fig. 4b). At such a high temperature of 169.5 °C, only a relatively small quantity of "nuclei" can be left in the melt to trigger subsequent SN crystallization of forming small spherulitic patterns. From Fig. 6(c), more detailed microstructure of elongated R-lamellae and large amounts of T-lamellae perpendicularly between R-lamellae can be observed, which is similar with the sample of S200-5. We also comparatively investigate the crystalline morphology of the sample after self-nucleating at 169.5 °C for 120 min (S169.5-120). In Fig. 6(d), it is interesting to find that, although the annealing time τ_s has increased to 120 min, S169.5-120 still retains a similar crystalline morphology as S169.5-5, including spherulite size and lamellae texture. These results suggest that, no matter how long it anneals at T_s, the number of the "nuclei" will not increases or decrease.

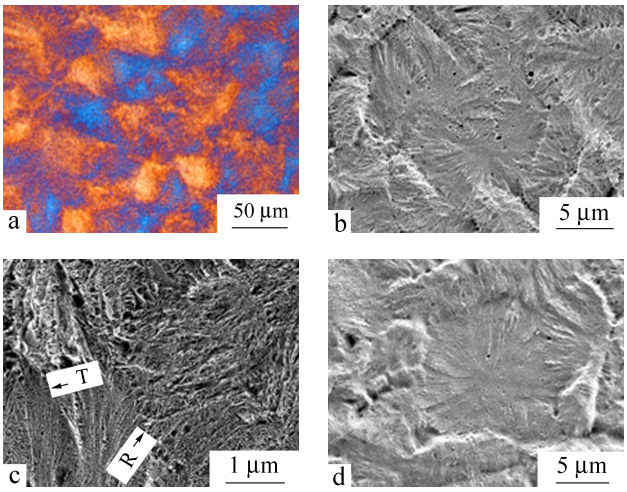


Fig. 6 (a) POM image of the sample after treated at 169.5 °C for 5 min (S169.5-5); (b) and (c) FESEM images of S169.5-5 at different magnifications; (d) FESEM image of the sample after thermally treated at 169.5 °C for 120 min (S169.5-120)

As T_s decreases to 168 °C with annealing for 5 min, only granular crystals can be seen by POM (Fig. 7a). When τ_s increased to 80 min, such morphology of numerous granular crystals remains the same for the sample of S168-80, as shown in the POM image of Fig. 7(b). FESEM images of S168-80 (Figs. 6c and 6d) manifest a different microstructure than the samples crystallized from the upper range of domain II (the samples of S169.5-5 and S169.5-120). It is noteworthy that the spherulitic patterns have disappeared, which should be ascribed to the increase in nucleation density. As calculated by Fillon *et al.*, SN increases the concentration of

nuclei by a factor of 10^6 than the blank sample, and when T_s decreases from upper range to the lower, the exponential increase in nucleation density will result in the spherulite diameter decreasing dramatically[2]. The lamellae texture of S168-80 represents a microstructure of numerous R-lamellae and lots of T-lamellae grow epitaxially on R-lamellae. We speculate that the "nuclei" in the melt crystallize into R-lamellae, while the remanent molecules are forced to grow epitaxially on R-lamellae, namely forming the T-lamellae. The thickness of R- and T-lamellae is both ~28 nm, thicker than that of "standard" sample. The thickened lamellae can be ascribed to the promoted crystallization of *i*PP with higher T_c, namely the SN effect in domain II.

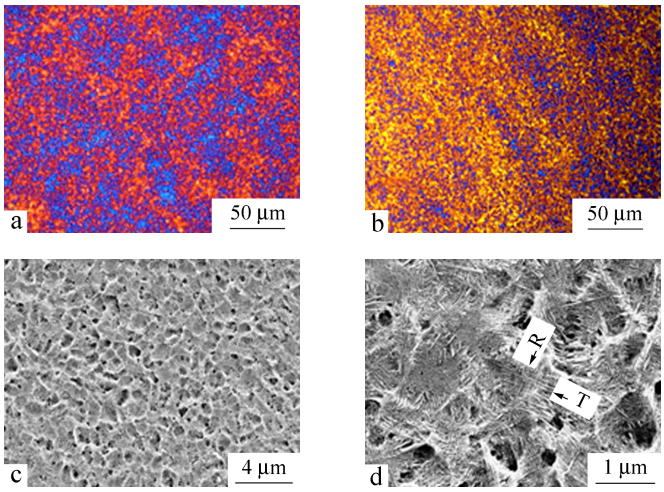


Fig. 7 POM images of the samples after treated at 168 °C for (a) 5 min (S168-5) and (b) for 80 min (S168-80); (c) and (d) FESEM images of S168-80 with different magnifications

From the observations above, as T_s decreases from higher to lower, we can show two apparently different crystalline structures after crystallized from upper and lower range of domain II: small spherulites in former; while granular crystals in latter. However, it is interesting to note that the samples crystallized from domain II have one feature in common: the crystalline morphologies only depend on T_s and won't be affected by τ_s. The time-independent crystallization morphologies can also be reflected in the results of DSC (Fig. 8). By comparing the DSC results of S169.5-5 and S169.5-120 in cooling run (Fig. 8a), the unshifted T_c at 125 °C indicates a constant nucleation density achieved on subsequent crystallization, which is independent of residence time spent at T_s. In addition, the re-melting curve and the value of T_{m1} are completely consistent with those of the sample after self-nucleating for 5 min (Fig. 8b). It seems that SN treatment at domain II could neither thermodynamically erase the memory of the pristine crystalline state nor kinetically alter the condition of the "nuclei" remaining at T_s. The invariable crystallization kinetics and morphology are the typical features of the samples after crystallizing from domain II.

If T_s is chosen in domain III ($T_s \leq 167$ °C), the subsequent crystallization features, including T_c and crystalline morphologies, are distinctly different from the samples crystallized from domains I and II. Now T_s is selected in the upper range of domain III, 167 °C as an example. Figure 9 presents the crystalline morphologies of the samples after thermally treated at 167 °C for 15 min (S167-15) and 120 min (S167-120). The morphology of S167-15 shows granular crystals (Fig. 9a) and S167-120 shows spherulites with weakly negatively birefringence (Fig. 9e), *i.e.* red color in I/III quadrants, blue in II/IV. It implies that after annealing at 167 °C for 120 min, the crystals seem to have recrystallized at annealing process. The lamellae evolution after annealing at 167 °C for different time is complementally investigated by using FESEM. Figures 9(b)–9(d) correspond to the microstructure of S167-15 and Figs. 9(f)–9(h) to that of S167-120. The sample only annealed for 15 min does not show any individual spherulites, but a "fish-bone" like morphology can be distinctly observed in Fig. 9(d). Such structure is similar to the case after crystallization from the lower range of domain II (the sample of

S168-80 in Fig. 7d). But further distinction can be recognized that S167-15 has longer R- but shorter T-lamellae than S168-80. Interestingly, as τ_s is prolonged to 120 min, the spherulitic pattern emerges in the microstructure morphology (Fig. 9f) and the contour of two adjacent spherulites are relatively clear in Fig. 9(g). The spherulites consist of almost all radially oriented R-lamellae, which is in accordance with the POM observation of negative birefringence. The lamellae thickness of S167-120 has been increased to nearly 40 nm (Fig. 9h), while that of S167-15 has only ~30 nm.

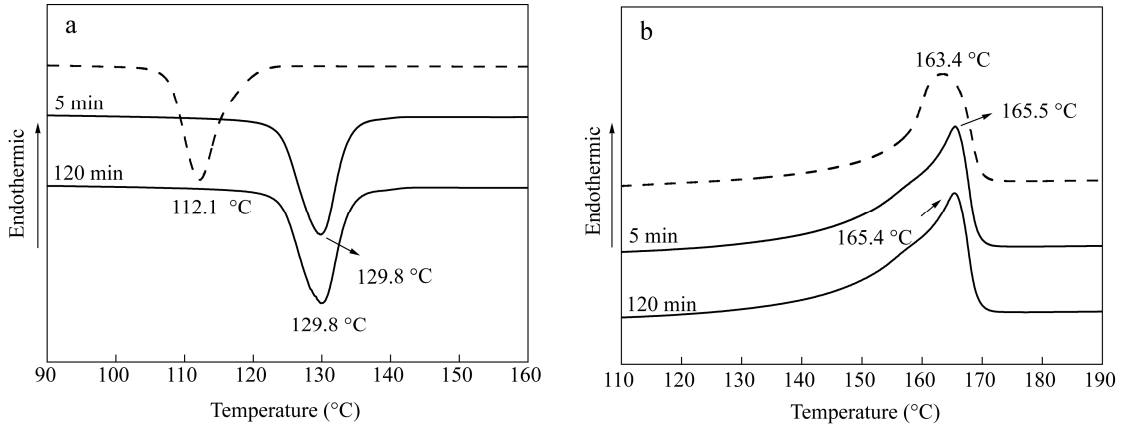


Fig. 8 (a) The crystallization curves of *i*PP after treated at 169.5 °C for 5 and 120 min; (b) Subsequent melting curves (Dash lines are the curves of "standard" sample for comparison.)

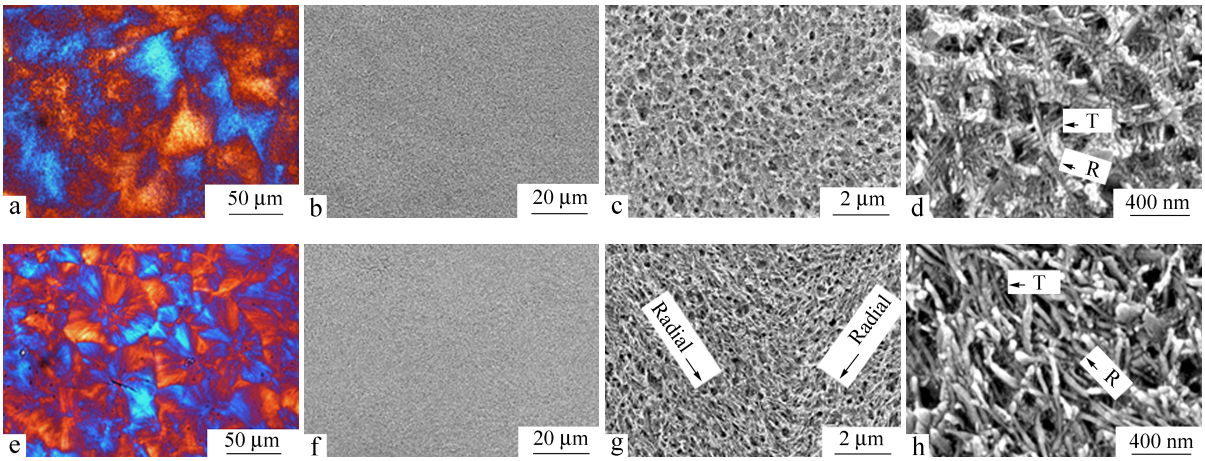


Fig. 9 (a)–(d) POM and FESEM images of the sample after treated at 167 °C for 15 min (S167-15); (e)–(h) the corresponding images of the sample after thermally treated at 167 °C for 120 min (S167-120)

In order to demonstrate the microstructure evolution more precisely, we monitor the recrystallization of *i*PP during the annealing process at 167 °C, which is presented as a serious of POM images (Fig. 10). The birefringence just disappears when the "standard" *i*PP reaches such a high temperature as 167 °C, while after annealing for 15 min, some spherulitic features are beginning to emerge (Fig. 10a). When the annealing time increases to 40 and 120 min, crystallization at 167 °C are gradually producing negatively birefringent sheaves of lamellae, which can be seen in Figs. 10(b) and 10(c). It is an extremely well-developed recrystallization of the remainder of the polymer that enables the isothermally crystallized spherulites to be clearly visible. The morphology evolution of the sample annealing at 167 °C provides convincing proof that the "nuclei" left at domain III will recrystallize to form longer and thicker R-lamellae as longer time spent at T_s. Recall the microstructure of the sample crystallized from domain II, it does not change after long time treatment at T_s,

keeping the invariable spherulite size and lamellae texture. It might be the different "nuclei" produced after treatment at domains II and III that trigger the different crystalline transformation. The specific nature of "nuclei" at domains II and III will be discussed in the next section.

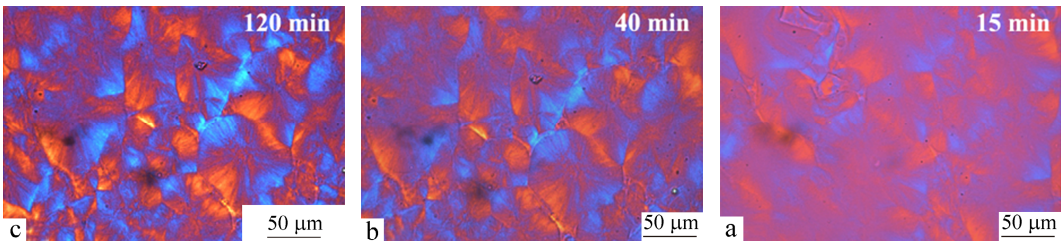


Fig. 10 POM images of the crystalline morphology of *i*PP annealed at 167 °C for various τ_s

Lastly, if T_s is selected in the lower part of domain III, partial melting occurs. Take the sample thermally treated at 164 °C for 5 min (S164-5) as an example. In POM image of S164-5 (Fig. 11a), the spherulite diameter is the same as the original "standard" *i*PP, indicating that the pristine spherulitic frame may persist at 164 °C. It is worth noting that S164-5 exhibits a strongly negative birefringence, indicating that R-lamellae take up a larger proportion than T-lamellae. In FESEM image of Fig. 11(b), distinct outline of spherulite can be observed. It should be emphasized that only when T_s locates in lower range of domain III can the "standard" spherulitic frame maintains; whereas in the upper range, the "standard" spherulitic frame will be destroyed due to the predominant melting process at T_s, leaving numerous crystal fragments in the melt. As shown in Fig. 11(c), the final spherulites of S164-5 consist of plenty of R-lamellae and a fraction of T-lamellae, which is in accordance with the negative birefringence observed by POM. It is surprising that the thickness of the R-lamellae developed by partially melting at 164 °C for just 5 min is considerably thicker than that of the "standard" sample (22 nm for "standard" and 47 nm for treated). This may be related to the fast reorganization of molten chains to form thicker and more 'perfect' lamellae at annealing process. During the heating process to 164 °C, the birefringence of initial "standard" *i*PP are gradually changing from mixed to negative, which can be proven by the direct observation in Fig. 12, indicating the fact that T-lamellae melt in advance of R-lamellae. The primarily melting

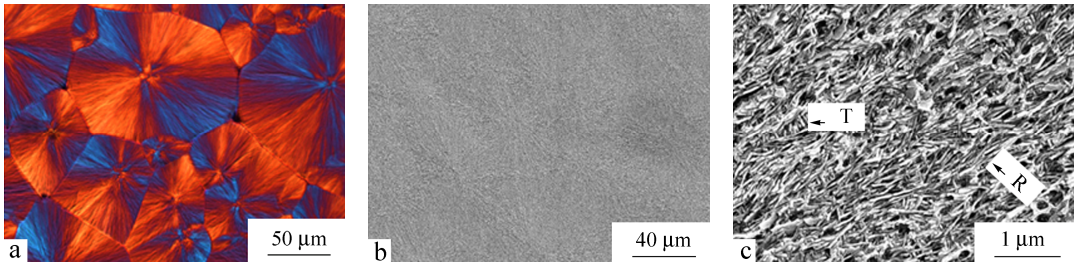


Fig. 11 Crystalline morphologies of the sample after thermally treated at 164 °C for 5 min (S164-5): (a) POM image; (b) and (c) FESEM images

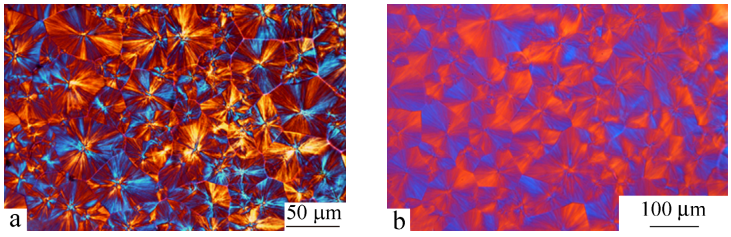


Fig. 12 Spherulite morphology of "standard" *i*PP (a) at 30 °C and (b) reheating to 163 °C at 10 K/min

of T-lamellae in the heating process can be ascribed to the higher density of defects in T-lamellae[32]. Thus, the R-lamellae dominated morphology of S164-5 in Fig. 11(a) is caused by the large proportion of R-lamellae left in the melt and thickened as annealing process goes, contributing to the final crystalline morphology with typically negative birefringence.

Based on the microstructure morphologies observed by FESEM, it is found that the lamellae morphology of the samples crystallized from domain III (including upper and lower ranges) presents a time-dependence evolution. As τ_s is increasing, the crystal fragments are recrystallizing to form longer and thicker R-lamellae, while reducing to form T-lamellae in the spherulites. Recall the DSC results of Fig. 3, the complementary analysis of crystallization and melting enthalpies is summarized in Table 1. The total exothermic enthalpy of crystallization ΔH_c decreases from 103.4 to 97.1 J/g as τ_s increases from 15 min to 120 min, which could be ascribed to the more recrystallization at annealing process and less at cooling process. In the heating run, T_{m2} is elevated from 176 °C to 181 °C (Fig. 3b) and ΔH_{f2} is significantly increased from 1.9 J/g to 10.3 J/g as τ_s increases, which are possibly related to the formation of thickened and prolonged R-lamellae during annealing at T_s. The features of the DSC curves in Fig. 13 provide supportive evidence for the speculation above. For T_s in the lower range of domain III, as τ_s is prolonged, double melting peaks will gradually merge into one annealing peak and negligible endotherm is detected upon subsequent crystallization, resulting in the crystal morphology composed of much more thickened R-lamellae and less T-lamellae, as shown in Fig. 9. Thus, it is reasonable to speculate that more R-lamellae are thickened during annealing process, the melting of which corresponds to the melting peak appeared at about 180 °C and contributes to the fusion enthalpy of ΔH_{f2}; the rest of molten chains mainly form T-lamellae under cooling run, the melting of which corresponds to the broad melting peak at about 167 °C and contributes to the endothermic enthalpy ΔH_{f1}.

Table 1. The crystallization and melting enthalpy of S167-15 and S167-120

Samples	ΔH_c (J/g)	ΔH_{c1} (J/g)	ΔH_{c2} (J/g)	ΔH_f (J/g)	ΔH_{f1} (J/g)	ΔH_{f2} (J/g)
S167-15	103.4	101.3	2.1	103.2	101.3	1.9
S167-120	97.1	89.1	8.0	107.3	97.0	10.3

ΔH_c: the total exothermic enthalpy of crystallization; ΔH_{c1}: the enthalpy of main crystallization peak at about 141 °C; ΔH_{c2}: the enthalpy of second crystallization peak at about 154 °C; ΔH_f: the total endothermic enthalpy of melting; ΔH_{f1}: the enthalpy of melting peak at about 167 °C; ΔH_{f2}: the enthalpy of second melting peak at about 180 °C

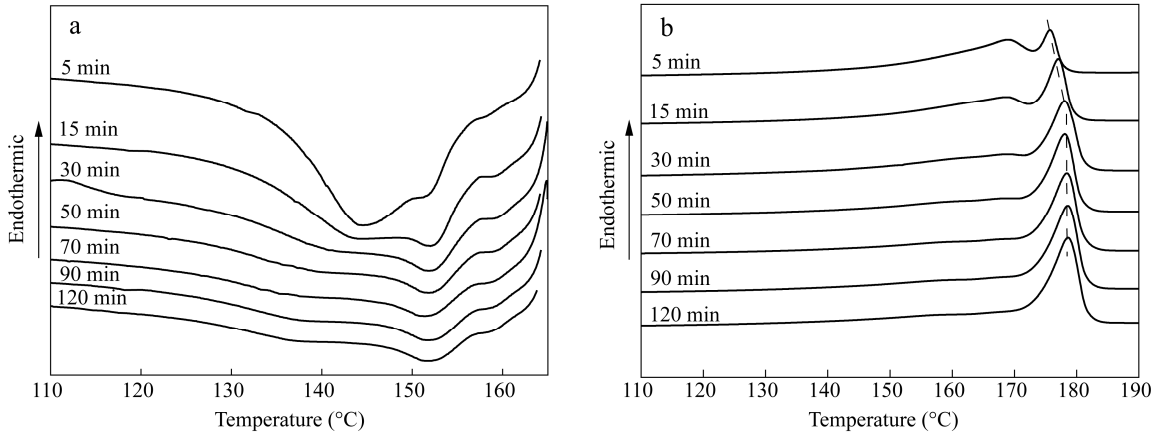


Fig. 13 (a) The crystallization curves of *i*PP after thermally treated at 165 °C for different τ_s and (b) subsequent melting curves

Schematic Illustration of Molten States of iPP at Various Domains

Based on the systematic analysis of microstructure of *i*PP crystallized from different T_s and the crystalline evolution during annealing process, we propose the probable models of the melt structures in the three domains. As known, complete or partial melting at high temperatures relies on a temperature-dependent balance between

the bulk melting of destroying crystalline regions and the thermally induced reorganization of molten into lamellae[33, 34]. In domain I, the "standard" *i*PP melts completely that all the fold molecules have enough mobility to reach a state of equilibrium, namely forming an entirely amorphous phase. Then in the cooling process, *i*PP crystallizes at the lowest T_c with no 'memory effect', creating large spherulites mainly composed of R-lamellae and a lot of vertically aligned T-lamellae, which agrees with the observation of mixed birefringence and lamellae microstructure of S200-5. The crystallization process from domain I is illustrated in Fig. 14.

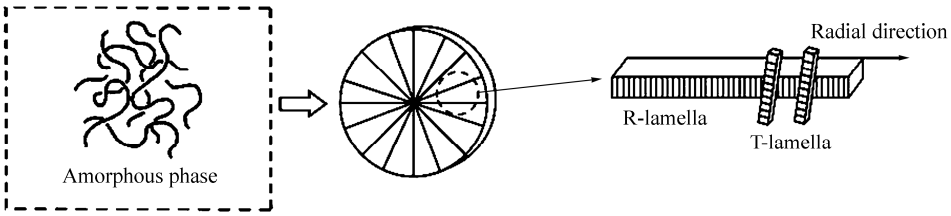


Fig. 14 Schematic illustration of *i*PP crystallized from domain I

In domain II, T_s is not high enough to erase all the thermal history of "standard" sample and several "nuclei" are retained in the melt, triggering subsequent SN effect with a prominently increased T_c. Fillon *et al.* considered that the self-nuclei survived in domain II were composed of crystal fragments that did anneal but never reached a size (or quantity) high enough for detection[2, 5]. However, Reid *et al*. reported that it was the residual sequence segregations that remained as the nuclei in the melt, which were unlikely to anneal[35–41]. Recently, Müller *et al*. summarized two possibilities of melt statuses in domain II: at higher temperature end of domain II, the melt retains some residual segmental orientation and at the lower end, small crystal fragments survive melting and constitute self-nuclei[13]. It has always been controversial about the nature of "nuclei" in domain II. In this study, we try to further understand the nature of "nuclei" in domain II from the perspective of crystalline morphologies. As discussed in the last section, the "nuclei" in domain II will not anneal or thicken at T_s, the crystallization kinetics and morphology of which are independent of the duration time; while the "nuclei" in domain III will suffer recrystallization to form longer and thicker R-lamellae, causing the time-dependent morphology evolution. It is the constant "nuclei", including the unchanged quantity and constitution, result in the unchanged crystalline morphologies and unshifted T_c after thermally treated for 5 or 120 min. We consider that the "nuclei" in domain II, both in the upper and lower ranges, are more likely to be a metastable state with locally ordered chains, instead of genuine "crystalline grains", which will not recrystallize as annealing treatment lasts. The rheological experiment shows the storage modulus and viscosity of the melt at domain II are the same as those at domain I (see Supporting Information, Fig. S1), which also confirm the conjecture that the "nuclei" kept at domain II behave in some way like mesomorphic phase, similar to the molten structure in domain I.

For a clear demonstration, a highly schematic, simple diagram of the melt structures in domain II is presented in Fig. 15. In the upper range of domain II, the number of "nuclei" is in relatively low amount, which will induce the subsequent crystallization of *i*PP to form numerous small spherulites (as shown in Fig. 6). As T_s enters in the lower range, these locally ordered chains accumulate to the critical quantity in the melt, and then lead to an entirely different crystalline morphology. Upon subsequent cooling, the randomly distributed "nuclei" crystallize into the short R-lamellae with the simultaneous nucleation of a large amount of T-lamellae growing perpendicularly to them (see Fig. 7d). The formation of T-lamellae was reported by Lotz *et al*. and they regarded it as a secondary crystallization process with epitaxial growth mechanism[42, 43]. We know that thermal treatments at elevated temperatures increase the mobility of chain molecules, which will lead the lamellae melting into amorphous phase; while the treatments at decreased temperatures hinder the diffusion of chain molecules, which is in favor of chain folding back upon lamellae. When T_s decreases from domain II to III, the effect of annealing (stabilization of nuclei) increases and the impact of melting decreases, which will gradually stabilize the crystal grains of pristine crystalline state. Theoretically, when T_s is in domain III, granular crystals will be left in the melt, which will be thickened since the polymer molecules tend to aggregate rather than diffuse into molten

phase. There must exist some equilibrium point between domains II and III, but determination of this temperature point is not the focus in this work.

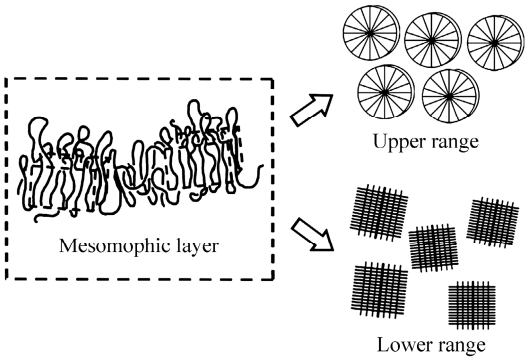


Fig. 15 Schematic illustration of *i*PP crystallized from domain II

In domain III, *i*PP preserves residual crystal fragments in the melt structure. The fragments of granular crystals or lamellae are dependent on the partially melting temperature T_s. The schematic of *i*PP crystallized from domain III for different annealing time is illustrated in Fig. 16. When T_s is selected in the upper range of domain III, only the residual blocks of granular crystal remain in the melt. Upon subsequent cooling, the rest of molten chains recrystallized on the existing lamellae, producing T-lamellae on the original lamellae. As shown in Fig. 9(d), the "fish-bone" like morphology can be observed by FESEM. However, if τ_s increases, possible aggregations or assemblies of crystal blocks will take place in the melt as annealing process goes (see Fig. 16), which are analogous to the Strobl's block mesostructure[36, 44]. The solidification transition and rapid lamellae rearrangements in the annealing process strengthen thermodynamically the stability of numerous crystal fragments, which do not happen to the locally ordered chains at domain II. During the annealing process, the molten chain segments will be attracted into crystalline to thicken R-lamellae, until the gain in free energy of crystallization *via* lamellae thickening is balanced locally due to the loss of entropy by the shortening of the segments in the amorphous region[45, 46]. If the annealing time is long enough, long R-lamellae will stack in the spherulite, and then cooling down with a small amount of T-lamellae growing orthogonally to the R-lamellae, which has been clearly confirmed by our results of a series of FESEM images (Fig. 9). For T_s in the lower range of domain III, the spherulitic frame of "standard" *i*PP cannot be destroyed, leaving the R-lamellae stack regularly in the radial orientation (the bottom in Fig. 16). The residual lamellae tend to reorganize and undergo annealing to form the thicker and more 'perfect' lamellae, forming the final spherulites with typically negative birefringence (see POM images of Fig. 10). The lamellae morphology of spherulites shows similar microstructure to the sample after long time treatment in the upper range of domain III, which has been described previously.

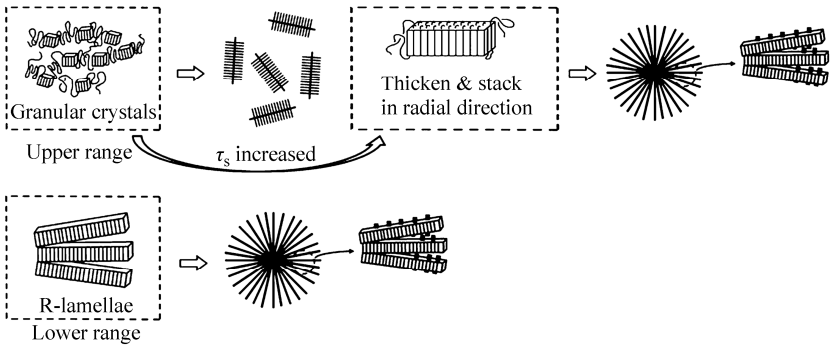


Fig. 16 Schematic illustration of *i*PP crystallized from domain III

The samples after partially melting and annealing in domain III show double melting peaks, which has been attracting broad interest from many studies[18, 45–49]. It has been found that in domain III, the formation of the annealing peak is a dynamic process with a time scale[45, 50]. Based upon the observations in previous section, we speculate that the melting behaviors of two peaks (T_{m1} and T_{m2}) observed by DSC should be associated with the melting of T-lamellae and R-lamellae, respectively. The rise of second melting point T_{m2} and enthalpy stems from the increasing number of thickened lamellae with the rearrangement of more molecule chains into R-lamellae during the annealing process at T_s. Additionally, we compared the melting curves of the samples after normal thermal procedure (as described in Fig. 1) and the samples being heated up directly after annealing at T_s, as shown in Fig. S2, which further evidences that the T_{m2} should be attributed to the melting of the lamellae produced at T_s rather than the cooling process. Furthermore, the values of T_{m2} exhibit a logarithmic time dependence (see Supporting Information, Fig. S3), $T_{m2} \propto \log(\tau_s)$. It implies that the thickness of R-lamellae correlates with τ_s in a form of a logarithmic dependence, indicating a continuous increase of lamellae thickness. Wang *et al*. considered such case of continuous thickening as a wedge-shaped growth profile at the lateral surface of lamellar crystals by dynamic Monte Carlo simulations[50]. Thus, we speculate that the annealing process of R-lamellae at T_s is a kind of wedge-shaped growth through the sliding diffusion of folded chains in the lamellae.

CONCLUSIONS

A detailed study on the features of crystalline morphologies of *i*PP, including spherulitic size, lamellae thickness and radial/tangential lamellae, *etc*., is performed to explore the melt structures of *i*PP in the three domains. Our study offers a further insight into the molten structures in the three domains and complements some understanding of self-nucleating and annealing. After *i*PP crystallized from domain I, the morphology of spherulites shows mixed birefringence, which is consistent with the "standard" sample. All the fold molecules have enough mobility to reach a state of equilibrium, namely forming entirely amorphous phase and *i*PP molecules form large spherulites mainly composed of R-lamellae and a lot of vertically aligned T-lamellae. After *i*PP crystallized from domain II, the crystalline morphologies are varying from small spherulites to randomly cross-hatched microstructures. The treatment in domain II could neither thermodynamically erase the memory of the pristine crystalline state nor kinetically alter the condition of the "nuclei" remaining at T_s, namely irrespective of the time. We attribute the "nuclei" to the structure of locally ordered chains, which cannot form genuine "crystalline grains". Thermal conditions at domain III preserve residual crystal fragments in the molten structure. The final crystalline structure is largely depend on the time spend at T_s, which differs from the feature of domain II. A possible aggregation or assemblies of crystal blocks happen to the melt as annealing process goes. The solidification transition and rapid lamellae rearrangements in the annealing process strengthen thermodynamically the stability of numerous crystal fragments, which do not happen to the locally ordered chains at domain II. When the annealing time is long enough, R-lamellae will stack in the spherulite, and then under cooling a small amount of T-lamellae grow orthogonally to the R-lamellae, resulting in the final spherulites of negative birefringence. In addition, based on the microstructures observed, the double melting endotherms appearing in DSC scans may correspond to the melting of R- and T- lamellae with different thickness.

REFERENCES

1 Cavallo, D., Gardella, L., Portale, G., Müller, A.J. and Alfonso, G.C., Polymer, 2014, 55(1): 137
2 Fillon, B., Wittmann, J.C., Lotz, B. and Thierry, A., J. Polym. Sci., Part B: Polym. Phys., 1993, 31(10): 1383
3 Xu, J.J., Ma, Y., Hu, W.B., Rehahn, M. and Reiter, G., Nat. Mater., 2009, 8(4): 348
4 Lorenzo, A.T., Arnal, M.L., Müller, A.J., de Fierro, A.B. and Abetz, V., Macromol. Chem. Phys., 2006, 207(1): 39

5 Lorenzo, A.T., Arnal M.L., Sanchez, J.J. and Müller, A.J., J. Polym. Sci., Part B: Polym. Phys., 2006, 44(12): 1738
6 Mamun, A., Umemoto, S., Okui, N. and Ishihara, N., Macromolecules, 2007, 40(17): 6296
7 Massa, M.V., Lee, M.S.M. and Dalnoki-Veress, K., J. Polym. Sci., Part B: Polym. Phys., 2005, 43(23): 3438
8 Müller, A.J., Hernandez, Z.H., Arnal, M.L. and Sanchez, J.J., Polym. Bull., 1997, 39(4): 465
9 Müller, A.J. and Arnal, M.L., Prog. Polym. Sci., 2005, 30(5): 559
10 Zhang, M., Lynch, D.T. and Wanke, S.E., Polymer, 2001, 42(7): 3067
11 Lorenzo, A.T., Arnal, M.L., Müller, A.J., Lin, M.C. and Chen, H.L., Macromol. Chem. Phys., 2011, 212(18): 2009
12 Chen, F., Shanks, R.A. and Amarasinghe, G., Polym. Int., 2004, 53(11): 1795
13 Müller, A.J., Michell, R.M., Pérez, R.A. and Lorenzo, A.T., Eur. Polym. J., 2015, 65: 132
14 Wang, Y.T., Lu, Y., Zhao, J.Y., Jiang, Z.Y. and Men, Y.F., Macromolecules, 2014, 47(24): 8653
15 Zhou, T.N., Yang, H., Ning, N.Y., Xiang, Y.F., Du, R.N. and Fu, Q., Chinese J. Polym. Sci., 2010, 28(1): 77
16 Maus, A., Hempel, E., Thurn-Albrecht, T. and Saalwachter, K., Eur. Phys. J. E, 2007, 23(1): 91
17 Kang, J., Chen, Z.F., Zhou, T., Yang, F., Chen, J.Y., Cao, Y. and Xiang, M., J. Polym. Res., 2014, 21(4): 384
18 Martins, J.A., Zhang, W.D. and Brito, A.M., Polymer, 2010, 51(18): 4185
19 Hamley, I.W., Parras, P., Castelletto, V., Castillo, R.V., Müller, A.J., Pollet, E., Dubois, P. and Martin, C.M., Macromol. Chem. Phys., 2006, 207(11): 941
20 Olley, R.H. and Bassett, D.C., Polymer, 1982, 23(12): 1707
21 Binsberg, F.l. and Delange, B.G.M., Polymer, 1968, 9(1): 23
22 Lugito, G., Yang, C.Y. and Woo, E.M., Macromolecules, 2014, 47(16): 5624
23 Wang, C., Chen, C.C., Cheng, Y.W., Liao, W.P. and Wang, M.L., Polymer, 2002, 43: 5271
24 Ye, H.M., Xu, J., Guo, B.H. and Iwata, T., Macromolecules, 2009, 42(3): 694
25 Wang, X.H. and Prud'homme, R.E., Macromol. Chem. Phys., 2011, 212(7): 691
26 Medellin-Rodriguez, F.J., Mata-Padilla, M., Sanchez-Valdes, S., Vega-Diaz, S. and Davalos-Montoya, O., J. Polym. Sci., Part B: Polym. Phys., 2008, 46(20): 2188
27 Li, X.Y., Ma, Z., Su, F.M., Tian, N., Ji, Y.X., Lu, J., Wang, Z. and Li, L.B., Chinese J. Polym. Sci., 2014, 32(9): 1224
28 Wu, C.M., Chen, M. and Karger-Kocsis, J., Polymer, 2001, 42(1): 199
29 Samuels, R.J., J. Polym. Sci., Part B: Polym. Phys., 1975, 13(7): 1417
30 Padden, F.J. and Keith, H.D., J. Appl. Polym. Phys., 1959, 30(10): 1479
31 Hosier, I.L., Alamo, R.G. and Lin, J.S., Polymer, 2004, 45(10): 3441
32 Yamada, K., Matsumoto, S., Tagashira, K. and Hikosaka, M., Polymer, 1998, 39(22): 5327
33 Gao, H.H., Wang, J., Schick, C., Toda, A., Zhou, D.S. and Hu, W.B., Polymer, 2014, 55(16): 4307
34 Viswanath, V., Maity, S., Bochinski, J.R., Clarke, L.I. and Gorga, R. E., Macromolecules, 2013, 46(21): 8596
35 Cho, K., Saheb, D.N., Choi, J. and Yang, H., Polymer, 2002, 43(4): 1407
36 Strobl, G., Prog. Polym. Sci., 2006, 31(4): 398
37 Kaji, K., Nishida, K., Kanaya, T., Matsuba, G., Konishi, T. and Imai, M., Adv. Polym. Sci., 2005, 191: 187
38 Li, L.B. and de Jeu, W.H., "Flow-induced mesophases in crystallizable polymers", Vol. 181, ed. by Abe, A., In Advances in Polymer Science, Springer-Verlag, Berlin, 2005, p.75
39 Cho, K., Saheb, D.N., Yang, H.C., Kang, B.I., Kim, J. and Lee, S.S., Polymer, 2003, 44(14): 4053
40 Reid, B.O., Vadlamudi, M., Mamun, A., Janani, H., Gao, H.H., Hu, W.B. and Alamo, R.G., Macromolecules, 2013, 46(16): 6485
41 Gao, H.H., Vadlamudi, M., Alamo, R.G. and Hu, W.B., Macromolecules, 2013, 46(16): 6498
42 Lotz, B., Wittmann, J.C. and Lovinger, A.J., Polymer, 1996, 37(22): 4979
43 Lotz, B. and Wittmann, J.C., J. Polym. Sci., Part B: Polym. Phys., 1986, 24(7): 1541
44 Stribeck, N., Nochel, U., Camarillo, A.A., Roth, S.V., Dommach, M. and Bosecke, P., Macromolecules, 2007, 40(13): 4535
45 Hingmann, R., Rieger, J. and Kersting, M., Macromolecules, 1995, 28(11): 3801
46 Rieger, J., Macromolecules, 1989, 22(12): 4540

47 Rochette, C.N., Rosenfeldt, S., Henzler, K., Polzer, F., Ballauff, M., Tong, Q., Mecking, S., Drechsler, M., Narayanan, T. and Harnau, L., Macromolecules, 2011, 44(12): 4845
48 Maiti, P., Hikosaka, M., Yamada, K., Toda, A. and Gu, F., Macromolecules, 2000, 33(24): 9069
49 Luo, F., Geng, C.Z., Wang, K., Deng, H., Chen, F., Fu, Q. and Na, B., Macromolecules, 2009, 42(23): 9325
50 Wang, M.Q., Gao, H.H., Zha, L.Y., Chen, E.Q. and Hu, W.B., Macromolecules, 2013, 46(1): 164